Journal of Hydrology 401 (2011) 240–249

Contents lists available at ScienceDirect

Journal of Hydrology

journal homepage: www.elsevier.com/locate/jhydrol

Relating TRMM Precipitation Radar backscatter to water stage in wetlands

Sumit Puri, Haroon Stephen, Sajjad Ahmad *

Department of Civil and Environmental Engineering, University of Nevada, Las Vegas, NV 89154, United States

ARTICLE INFO

Article history:
Received 7 October 2010
Received in revised form 3 February 2011
Accepted 21 February 2011
Available online 26 February 2011

This manuscript was handled by
K. Georgakakos, Editor-in-Chief, with the
assistance of V. Lakshmi, Associate Editor

Keywords:
TRMMPR
Water stage
Wetlands
South Florida

SUMMARY

Information on water stage over an extended area is important for hydrological and ecological studies. Microwave remote sensing provides an opportunity to measure changes in water stage from space because of its sensitivity to land surface characteristics; it reduces the need to monitor water stage at multiple locations. In this research, a linear model is developed which relates variation in water stage measurements (w_s) to Tropical Rainfall Measuring Mission Precipitation Radar backscatter (σ°). The estimated water stage from the model is compared with the observed water stage in the wetlands of South Florida. The model performance is assessed by comparing the correlation coefficient (R), the root mean square error (RMSE), and the non-exceedance probability of mean absolute error between observed and modeled water stage measurements for various landcovers. The model works reasonably well in the regions with tree heights greater than 5 m. For example, over woodlands R ranges between 0.59–0.93 and the average RMSE = 19.8 cm. Similarly, for wooded grassland, R ranges between 0.54–0.93 and the average RMSE = 19.8 cm. For other relatively shorter height vegetation landcovers such as grassland (R = 0.57–0.85, RMSE = 20.1 cm) and cropland (R = 0.69–0.79, RMSE = 18.2 cm), the model also performs reasonably well. The research presents a novel use of TRMMPR data and gives an insight into the effect of water level in partially inundated vegetation on radar backscatter.

1. Introduction

A wetland is an area where the soil is saturated seasonally or perennially resulting in shallow pools of standing waters. Wetlands have the ability to store floodwater and protect shoreline (Brande, 1980). They play an important role in flood control, contaminant attenuation, and carbon sequestration (McAllister et al., 2000; Pant et al., 2003). They also impact the regional ecology and hydrological cycle.

Understanding the hydrological processes in wetlands is important because it helps develop measures to maintain ecological functions, and it protects the economic benefits of the wetlands (Ozesmi and Bauer, 2002). In particular, it is necessary to understand the changes in water stage as this affects the water flow path between the surface and ground water (Johnson et al., 2004). Changes in water stage have been linked to changes in salinity in the wetlands (Gorham et al., 1983), which can modify the vegetation patterns.

Water stage in wetlands needs to be monitored because of its consequential impact on the surrounding environment. However, due to a wide expanse of wetlands and a lack of hydrological surveys, some wetlands are rarely monitored (Zhang, 2008). A method for water stage estimation needs to be developed to compliment the available ground measures.

Understanding the changes in water stage over time is important for hydrological modeling (Ahmad and Simonovic, 2001; Mosquera-Machado and Ahmad, 2007) and an appreciation of the wetland ecosystem (Bourgeau-Chavez et al., 2005). Several techniques using in situ observations have been used in the past, and these techniques usually involve comparing surface water heights to a given vertical reference level. For example, water stage in streams has been derived from Rating Curves which provide a functional relationship between stage and stream discharge.

In addition to Rating Curves, other methods have been used to track water stage. Several studies have monitored water stage using Synthetic Aperture Radar (Bourgeau-Chavez et al., 2005; Kasischke and Bourgeau-Chavez, 1997; Kasischke et al., 2003), passive microwave sensors (Sippel et al., 1998), and Landsat thematic mapper (Mertes et al., 1995). Researchers have also used Interferometric Synthetic Aperture Radar (Hong et al., in press, 2010; Wdowinski et al., 2004, 2008) and airborne scanning laser altimetry to estimate water surface elevation and extent during flooding (Mason et al., 2007).

Remote sensing of water level in large water bodies is an active area of research and application. For example, altimeters are primarily designed to measure the height of the ocean's surface, but they have also been used to measure surface water stage. However, there have been problems with the accuracy of measurements using altimeters; prior studies have reported discrepancies up to several meters when surface water stage is measured (Birkett et al., 2002; Calmant et al., 2008). Another area of developing

* Corresponding author. Tel.: +1 702 895 5456.
E-mail address: sajjad.ahmad@unlv.edu (S. Ahmad).

0022-1694/$ - see front matter © 2011 Elsevier B.V. All rights reserved.
doi:10.1016/j.jhydrol.2011.02.026

research is Surface Water Ocean Topography (SWOT). SWOT satellite mission will be launched by NASA in 2020 and has the hydrologic objective of providing a global inventory of terrestrial water surface bodies (rivers, lakes, wetlands) with area >50 m^2 and rivers with width more than 100 m (Alsdorf et al., 2003).

Measuring water stage using remote sensing is possible because of the double bounce from the vertical parts of the vegetation (e.g., tree trunks) in the presence of horizontal water surface (Richards et al., 1987). The transmitted radar signal after undergoing a double bounce from tree trunks and water surface is reflected back to the sensor. However, the signal undergoes two way path attenuation due to volume scattering by the canopy. Thus, changes in the water level are reflected in the strength of the backscatter signal due to effect of variations in the two way path attenuation. For example, water in a non-vegetated area or over a completely submerged vegetation area causes mostly specular reflection of the transmitted radar signal (except under high wind conditions).

Land surface backscatter (σ°) is sensitive to physical and dielectric characteristics of the target area. Physical characteristics such as surface roughness and dielectric characteristics such as water content can impact land surface backscatter. The surface roughness is governed by the geometric features of soil (relief) and soil cover (vegetation). As a result, water in the presence of vegetation contributes to the roughness characteristics of the surface. In the case of open water, incident radiation undergoes specular reflection; whereas over vegetation, changes in water depth alter roughness characteristics. Roughness characteristics are changed through the partial submergence/exposure of the vegetation trunk/canopy which impacts the scattering behavior of the incident radiation. A better understanding of these phenomena in wetlands can be used to develop a relationship between water stage and backscatter.

In this paper, we present a method to estimate water stage (w_s) using the Tropical Rainfall Measuring Mission Precipitation Radar (TRMMPR) backscatter data. Use of TRMMPR backscatter is tested for the first time to estimate water stage. A model is developed that relates w_s measurements to backscatter. The effect of vegetation greenness on model performance is investigated by incorporating the Normalized Difference Vegetation Index (NDVI) into the model as a measure of greenness of the vegetation. The model is tested in wetlands of South Florida.

This paper is organized as follows: Section 2 describes the study area and data sets used in this research; Section 3 presents the w_s model and model parameters. The comparison between estimated and observed w_s is discussed in Section 4. Finally, Section 5 presents conclusions.

2. Study area and data description

This section describes the study area and data sets used in this research. The Tropical Rainfall Measuring Mission specifications, measurement of water stage and characteristics of Normalized Difference Vegetation Index are described. The acquisition procedure for each of the datasets is also discussed.

2.1. South Florida wetlands

The South Florida region as shown in Fig. 1a is characterized by flat topography and average annual rainfall of about 1300 mm/yr (Alaa et al., 2000). The Everglades National Park (ENP), located in South Florida, consists mostly of wetlands (Doren et al., 1999) and covers an area of 6110 km^2. The water bodies and lakes in South Florida experience significant changes in the seasonal and interannual cycle of water stage because of the variability in climate.

This region has a large number of man made levees and water control structures. The Everglades Agricultural Area (EAA) of South

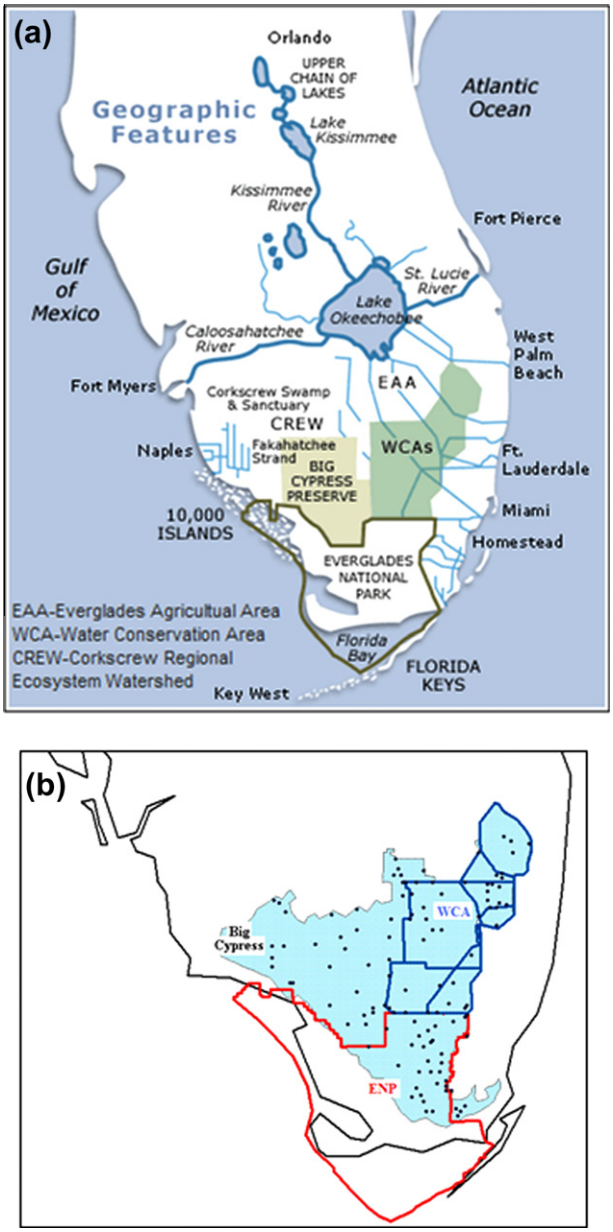

Fig. 1. (a) Map showing study area in South Florida (*Source*: SFWMD website). (b) Location of stations in a GIS map.

Florida lies to the south of the Lake Okeechobee (Vedawan et al., 2008). Adjacent to EAA are the Water Conservation Areas (WCAs) that store the surplus water in the region. Everglades National Park that lies to the south of WCAs also has tropical and sub-tropical forests (Cavender and Raper, 1968).

In certain areas, mainly WCAs, the operation of the flood control structures result in the accumulation of water exceeding natural levels (Wdowinski et al., 2008). Therefore, it is important to monitor water stage in order to understand the hydrological flow in wetlands. There are 114 water measuring stations that lie in the wetland regions of ENP, WCAs, and Big Cypress as depicted in Fig. 1b. These sites represent diverse land use categories summarized in Table 1.

2.2. Tropical Rainfall Measuring Mission Precipitation Radar

TRMM Precipitation Radar (TRMMPR) aboard TRMM satellite was designed to provide information about rainfall distribution

Table 1
Description of landuse categories (Hansen et al., 2000).

Landuse category	Tree height (m)	Canopy cover	Number of stage sites
Woodland	>5	40% < tree canopy < 60%	22
Wooded grassland	>5	10% < tree canopy < 40%	20
Closed shrubland	<5	Bush/shrub > 40%	15
Open shrubland	<2	10% < canopy cover < 40%	17
Grassland	–	Herbaceous cover	36
Cropland	–	Crop producing fields	4
Total			114

in the tropical and sub-tropical regions (Kummerow et al., 1998). TRMM operates in a 350-km circular orbit with an inclination of 35°. Precipitation Radar, operating at 13.8 GHz (*Ku*-band; 2.2 cm wavelength) and Horizontal transmit and receive (HH) polarization has a cross track scan angle of 0° (nadir) to 17° with a swath width of 215 km and a cross range spatial resolution of 4.4 km. In order to extend the mission life, satellite altitude was increased to 402.5 km which resulted in an increased ground resolution of 5 km.

TRMMPR measurements have been used to study vegetation (Stephen and Long, 2002; Satake and Hanado, 2004), deserts (Stephen and Long, 2005), and ocean winds (Li et al., 2004). In August 2001, TRMMPR's design objective was to provide a three dimensional structure of rain with a vertical resolution of 250 m (Kozu et al., 2001). Nevertheless, previous research has shown its usefulness to study characteristics of land surfaces. TRMMPR measurements have shown to be sensitive to the surface soil moisture (Seto et al., 2003; Narayan et al., 2006; Stephen et al., 2010; Ahmad et al., 2010).

Although horizontal polarization has greater penetration into the vertical vegetation stand, the high frequency of *Ku*-band is subject to greater attenuation by the plant leaves and branches. Nevertheless, the large footprint (4.4 km) allows sufficient surface coverage to study the effects of phenomena under the vegetation canopy. Small random gaps in the vegetation where incident waves can reach the lower levels result in backscatter values dependent on the characteristics of the lower levels of canopy, vegetation, and water.

TRMMPR data is available at an irregular temporal and spatial grid for the tropical region lying within 36°N to 36°S. The backscatter images of the study area are produced from this data for a time interval for which sufficient backscatter information is available over the study area.

Backscatter measurements from multiple orbits are combined at each grid point to produce backscatter images. Since combining multiple orbits results in backscatter data collected at different incidence angles, a linear model between backscatter and incidence angle is used. In this model, a reference incidence angle of 10° is used to determine the normalized backscatter at each grid cell. Thus, images of backscatter normalized to a 10° incidence angle are prepared. TRMMPR measurements from a 14 day time interval are sufficient to prepare an acceptable image. Thus, normalized backscatter (**A**) images are prepared for 14 days with a moving window of 7 days. Each pixel in the image corresponds to 2×2 km area of the land surface. The higher resolution is achieved by deconvolving the backscatter measurements using the antenna response function of TRMM Precipitation Radar. A median filter is applied to remove the noise from the images produced with this method.

Each TRMMPR backscatter measurement is provided along with a rain flag which is set if rain was detected in the measurement cell. In order to remove the effect of rain on the results of this research, backscatter measurements contaminated by rain are not used.

2.3. Normalized difference vegetation index

NDVI is the normalized difference between infrared band and visible band reflectivities, and it is used to monitor vegetation (Tucker, 1979). It is a numerical index that ranges between −1.0 to +1.0 and represents greenness of vegetation. It is highly correlated with other vegetation parameters like leaf area index and canopy cover and thus serves as a good descriptor for vegetation discrimination (Gao et al., 2002). High values that are close to 1.0 represent dense vegetation and forests, whereas low values (0.2–0.4) indicate the presence of shrubs and grasslands.

NDVI data is derived from AVHRR and acquired from Earth Explorer website (http://edcsns17.cr.usgs.gov/EarthExplorer/) maintained by the United States Geological Survey. It is available at 1 km spatial resolution. A 3×3 cell is averaged to obtain NDVI at the same spatial resolution as TRMMPR σ°. The 14-day NDVI composites at 7-day time steps are acquired for the time period 1998–2008. There are a total of 52 NDVI composites for each year. Images with excessive cloud cover were removed before the analysis.

2.4. Water stage data

The water stage data for this research is obtained from South Florida Water Management District (SFWMD) online database for the time period 1998–2008. SFWMD monitors a network of control stations that provide daily average estimates of water level, rainfall, and other key hydrologic parameters. The stage data consists of daily average water levels above the National Geodetic Vertical Datum of 1929 (NGVD29).

Most of the stage measurement stations are located near the water control structures for logistical and operational reasons (Wdowinski et al., 2008). As a result, the interiors of natural flow wetlands are sparsely monitored. Water stage measurements are averaged over a 14-day period with a 7-day moving window to match the temporal resolution of the TRMMPR normalized backscatter.

3. Model description

TRMMPR backscatter depends on vegetation characteristics, moisture content, and surface roughness. This section describes an empirical model that relates σ° to water stage. Backscatter measurements are affected by incidence angle (θ). A typical σ°–θ plot for incidence angle range of 3° to 15° is shown in Fig. 2. The relative contribution from surface and vegetation scattering depends on the vegetation density and is reflected in the slope of the σ°–θ relationship. It is approximated to be linear for angles between the given incidence angle range. The σ°–θ is modeled as

$$\sigma^\circ = \mathbf{A} + \mathbf{B} \cdot (\theta - \theta_{ref}) \quad (1)$$

where θ_{ref} is the reference angle, **A** (dB (decibels)) is the backscatter normalized to θ_{ref} and **B** (dB/°) is the slope of the line fit. The reference incidence angle θ_{ref} is chosen to be 10° because σ° at this angle is sensitive to soil moisture (Ulaby and Batlivala, 1976). Although this high sensitivity is observed for L- and C-band backscatter, Ku-band backscatter has shown good sensitivity to soil moisture in Lower Colorado River basin (Stephen et al., 2010).

In this research, σ° measurements from multiple orbits are used to prepare images of backscatter normalized to 10°. Study area is gridded into 2×2 km cells and for each cell Eq. (1) is used to compute the **A** using backscatter measurements from multiple orbits. The antenna response function is used to deconvolve the

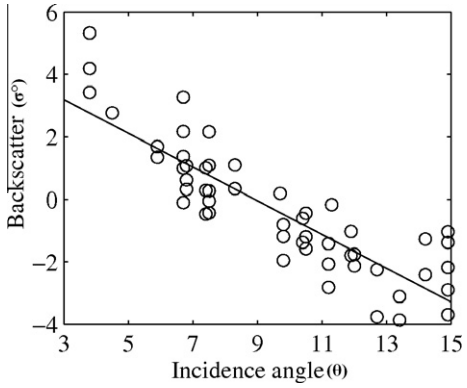

Fig. 2. General behavior of σ°–θ response.

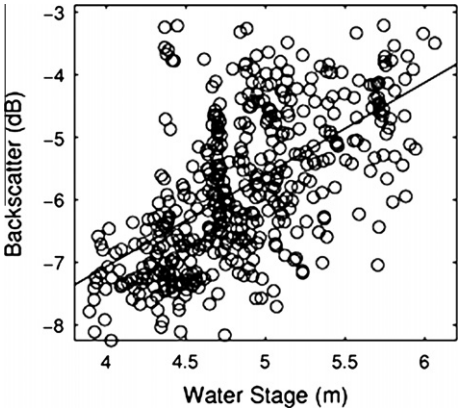

Fig. 4. Variation of backscatter with water stage for a site in Big Cypress area.

measurements to acquire high resolution images. The Eq. (1) model fitting and deconvolution are performed simultaneously where the linear regression is performed using measured backscatter weighted by the value of antenna response for the given cell.

Fig. 3 is the **A** image of South Florida and illustrates the variation in **A** due to surface characteristics. Rough surface areas such as mountain ranges have higher backscatter (bright spots) compared to smoother surfaces such as plains. Large urban areas, major cities, and riparian areas with dense vegetation also appear as bright areas with high backscatter.

In the case of partially inundated vegetation, **A** depends on the characteristics of the water surface roughness governed by wind conditions. The effect of wind conditions is not considered in this research.

TRMM backscatter depends on the amount of partially submerged vegetation. In the areas with high water stage (submerged vegetation), the water surface is typically smooth which results in specular reflection of the incident radiation. The specular reflection results in low backscatter. It is noted that for nadir (vertical) view, i.e. $\theta = 0^{\circ}$ (not considered in this research), the specular reflection would be directed back to the sensor. In the areas where the height of vegetation is greater than the water stage, the backscatter signal depends on the extent of submerged vegetation. This principle is used to estimate the effect of water stage on σ° measurements.

Fig. 4 shows the dependence of backscatter on the water stage for a site in the Big Cypress area. The relationship between backscatter and water stage depends on the stature of the vegetation relative to the water stage change as well as the ability of the electromagnetic radiation to penetrate the vegetation. As the water stage increases, the backscatter also increases, which demonstrates a linear relationship. This inter-dependence between w_s and **A** is modeled by

$$w_s(\mathbf{A}) = \boldsymbol{\mu}_{\mathbf{s}} + \mathbf{T} \cdot \mathbf{A} \tag{2}$$

where w_s is water stage in m. $\boldsymbol{\mu}_{\mathbf{s}}$ and **T** are the calibration parameters in (m) and (m/dB)) respectively. $\boldsymbol{\mu}_{\mathbf{s}}$ is the average value of water stage and **T** is the parameter relating w_s and **A**.

For each site, w_s and **A** data are used to compute the model parameters $\boldsymbol{\mu}_{\mathbf{s}}$ and **T** by minimizing the root mean square error (RMSE) between observed and modeled w_s. Seventy-five percent of the data is used to obtain model parameters $\boldsymbol{\mu}_{\mathbf{s}}$ and **T**. These model parameters are used to compute w_s from the remaining 25% of the data. The validation process consists of comparing the w_s values obtained from the model with the observed water stage values. The correlation coefficient (R), RMSE, and non-exceedance probability are computed between observed and modeled water stages, and the accuracy of the model estimates is assessed. Box plots are used to compare the distribution of observed data and model predictions.

In order to obtain a better understanding of the role of vegetation in the proposed model, NDVI is added into the model, as given by

$$w_s(\mathbf{A}, \mathrm{NDVI}) = \boldsymbol{\mu}_{\mathbf{s}} + \mathbf{T} \cdot \mathbf{A} + \mathbf{P} \cdot (\mathrm{NDVI} - \mu_{ndvi}) \tag{3}$$

where **P** is the weighing factor describing the effect of NDVI and μ_{ndvi} is the average NDVI over the calibration period.

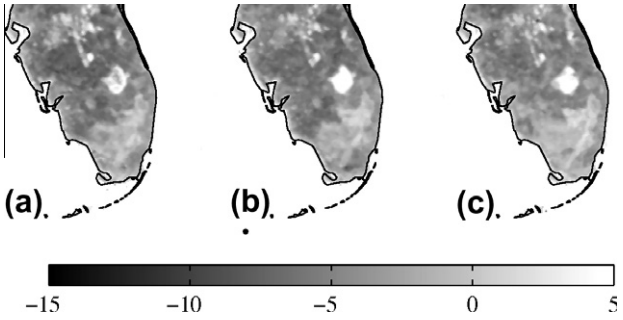

Fig. 3. TRMMPR normalized backscatter (**A**) image of South Florida during (a) January 1, 2008–January 14, 2008; (b) June 7, 2008–June 21, 2008; (c) September 14, 2008–September 28, 2008.

4. Results

The model is applied to the data over various land use types and the results are reported in this section. Different land use classes were identified using the University of Maryland's 1 km Global Land Cover Product (Hansen et al., 2000) available at http://www.geog.umd.edu/landcover/1km-map.html. Over each landuse, a representative site is selected and time-series plots consisting of observed and modeled water stage are discussed. The scatterplot and non-exceedance probability plot of absolute error are presented. In addition, scatterplots, non-exceedance probability plots, and boxplots are presented to show the overall performance for each landuse type. A summary of model performance parameters (R, RMSE) for all landuse categories is provided in Table 2.

Fig. 5 shows the results of the water stage model applied to the woodland area for the testing period of 3 years. Woodland is characterized by having canopy cover between 40% and 60% and tree height greater than 5 m. The peak water stage for woodlands is 4.9 m.

Fig. 5a shows the time-series plot of observed and modeled water stage. The variation in water stage is related to rainfall events or operation of control gates in the region.

Table 2
Model performance for various landuse types.

Landuse	Number of sites	*R*	RMSE (cm)	Percentage of estimates with error <15 cm (%)	Percentage of estimates with error <30 cm (%)
Woodland	22	0.59–0.93	19.8	66.6	91.0
Wooded grassland	20	0.54–0.93	19.8	73.2	93.7
Closed shrubland	15	0.55–0.96	16.1	72.1	94.3
Open shrubland	17	0.57–0.84	17.3	70.0	93.2
Grassland	36	0.57–0.85	20.1	71.1	92.1
Cropland	4	0.69–0.79	18.2	67.3	91.9

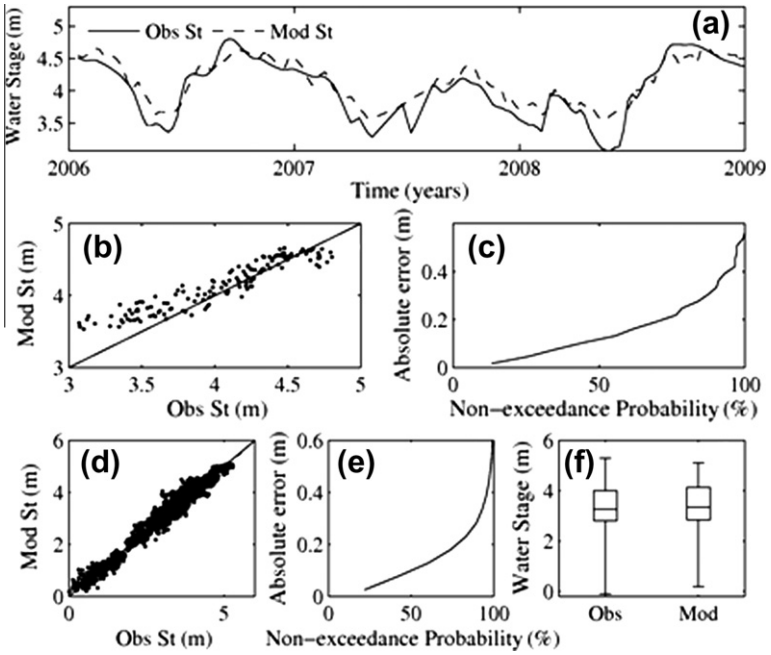

Fig. 5. Water stage model as applied to wetlands in woodland: (a) time-series plot of observed and modeled water stage, (b) scatterplot of observed and modeled water stage, (c) non-exceedance probability plot, (d) combined scatterplot of observed and modeled water stage for all the woodland sites, (e) combined non-exceedance probability plot, and (f) boxplot distribution of observed and modeled water stage.

The model is able to capture the variation in water stage reasonably well. The modeled water stage, in general, follows the high and low variations except in summer months. During the summer months, the model over-estimates the low values.

Fig. 5b shows the scatterplot of observed and modeled water stage where $R = 0.93$ and RMSE = 21.3 cm. Over-estimation of stage is indicated by the data points above the 45° line (line with slope = 1) whereas the points below the line indicate under-estimations. It is evident in Fig. 5b that for the selected woodland site in the Big Cypress Preserve, the model over-estimates the low values of water stage.

Fig. 5c is the non-exceedance probability plot where the *x*-axis is the probability of getting an absolute error corresponding to a value on the *y*-axis. For example, 59.7% of the modeled water stage values have an error of 15 cm or less and 85.8% have an error of 30 cm or less. The TRMMPR backscatter successfully captures the variation in exposed vegetation due to the rise and fall of water stage in the area.

In order to analyze the overall behavior of the model, data from all 22 woodland sites is combined in the ensemble of scatterplot, non-exceedance probability, and boxplot shown in Fig. 5d–f. The correlation coefficient for 22 woodland sites ranges between 0.59 and 0.93, and the average RMSE for all sites is 19.8 cm, indicating that the model works well over woodlands. Moreover, in the non-exceedance probability plot [Fig. 5e], 66.6% of data points have an error of 15 cm or less and 91% of data points have an error of 30 cm or less.

Fig. 5f is a boxplot of the distribution of observed and modeled water stage. The upper and lower edges of the box correspond to the 75th and 25th percentile of the data. The horizontal line between the box is the median of the data set. The 95th percentile and 5th percentile are shown by whiskers above and below the box. The boxplot shows that the distributions of observed and modeled water stage are similar.

Fig. 6 shows the time-series plots of observed and modeled water stage for a representative point in each of the landuse categories for the testing period. The *y*-axis of the figures shows water stage, and it is different for each sub-plot because the range of water stage variation differs largely from one landuse to the other. Woodland and wooded grassland have 3 years of testing data available whereas shrubland (closed and open) have 2 years of testing data. Grassland and cropland have one and a half years of testing data.

The time-series plots for the six landuses follow similar patterns. They all show a decline in water stage values during the summer months. This can be attributed to high evapotranspiration during these months. With exception of the grassland and cropland, where maximum stage value is less than 2 m, water stage in other landuses reaches up to 4 m.

Fig. 6b shows the time-series plot for a representative point in wooded grassland. Wooded grassland is characterized by tree

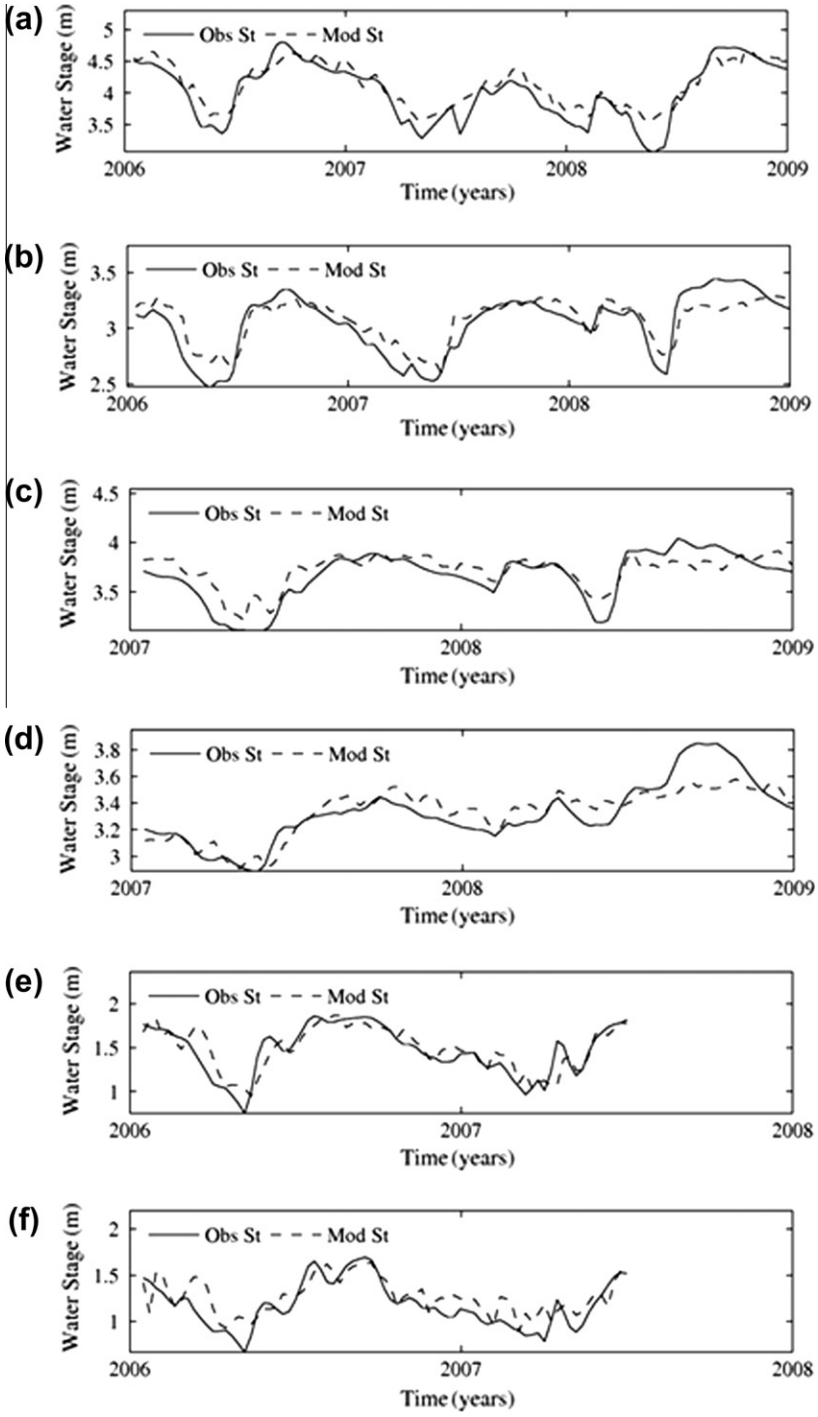

Fig. 6. Time-series plots of observed and modeled water stage in (a) woodland, (b) wooded grassland, (c) closed shrubland, (d) open shrubland, (e) grassland, and (f) cropland.

canopy cover between 10% and 40% and tree heights greater than 5 m. The model over-estimates the lower values of stage and underestimates the higher stage values as observed in March, 2006 and November, 2008.

The time-series plot for a representative site of closed shrubland is shown in Fig. 6c. Closed shrubland has greater than 40% canopy cover and is dominated by shrubs that are less than 5 m in height. Most of the water stage at various sites in closed shrubland is less than 5 m which does not result in specular reflection of incident radiations because the height of vegetation is shorter.

Fig. 6d shows the time-series plot for a point in open shrubland. Open shrubland consists of tree with height less than 2 m and canopy cover is between 10% and 40%. It is observed that the model does not capture the high values of water stage that occurred during the end of the year 2008.

The observed and modeled water stage plots for one and a half years of testing data for grassland and cropland is shown in Fig. 6e and f, respectively. Grassland is covered with continuous herbaceous cover consisting of less than 10% tree canopy cover whereas; in cropland, more than 80% of landscape is covered with crop producing fields. Therefore, the maximum water stage in this landuse is below 2 m. In both these landuses, the modeled water stage follows the patterns of observed water stage and captures its rise and fall variation.

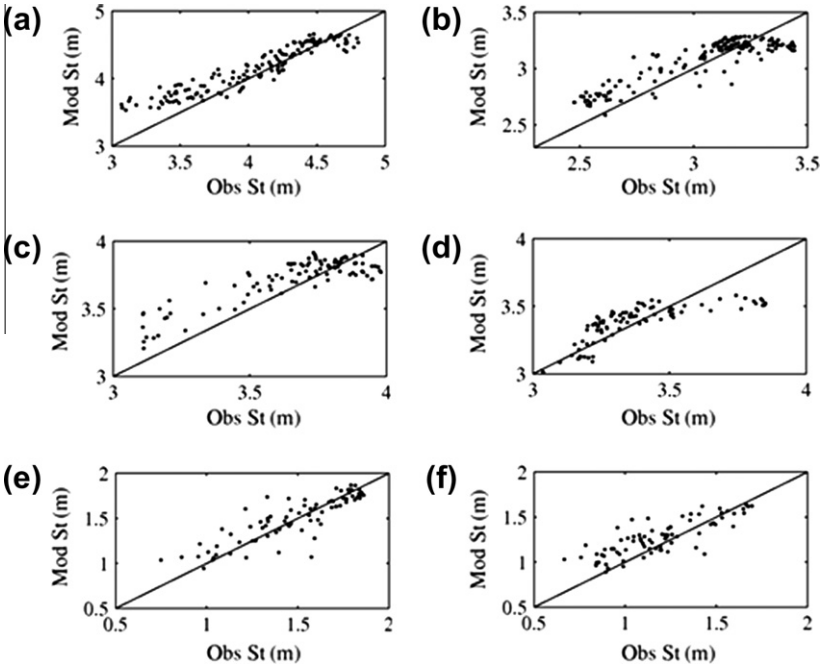

Fig. 7. Scatterplot of observed and modeled water stage for a representative site in (a) woodland, (b) wooded grassland, (c) closed shrubland, (d) open shrubland, (e) grassland, and (f) cropland.

Fig. 7 shows the scatterplot of observed and modeled water stage for representative site in all the six landuses. Fig. 7b shows the scatterplot for wooded grassland. The model captures the variation in water stage with $R = 0.89$ and RMSE = 14.3 cm. The model also works well for closed shrubland capturing the highs and lows of the water stage variation with $R = 0.86$ and RMSE = 15.5 cm [Fig. 7c]. The scatterplot results for open shrubland is shown in Fig. 7d and has $R = 0.84$ and RMSE = 12.8 cm. The scatterplots for grassland and cropland are shown in Fig. 7e and f, respectively. The R for representative site in grassland is $R = 0.85$ whereas; RMSE = 15.8 cm. The same for site in cropland is $R = 0.79$ and RMSE = 18.0 cm.

The non-exceedance probability for the six landuse types is shown in Fig. 8. Fig. 8b for wooded grassland indicates that 99.3% of the estimates have an absolute error of 30 cm or less. The non-exceedance plot for closed shrubland in Fig. 8c shows that 66.9% of the water level estimates have an absolute error of 15 cm or less, and 95.4% of the estimates have an absolute error of 30 cm or less. For open shrublands, the non-exceedance probability plot shown in Fig. 8d indicates that 84.9% of the estimates have an error

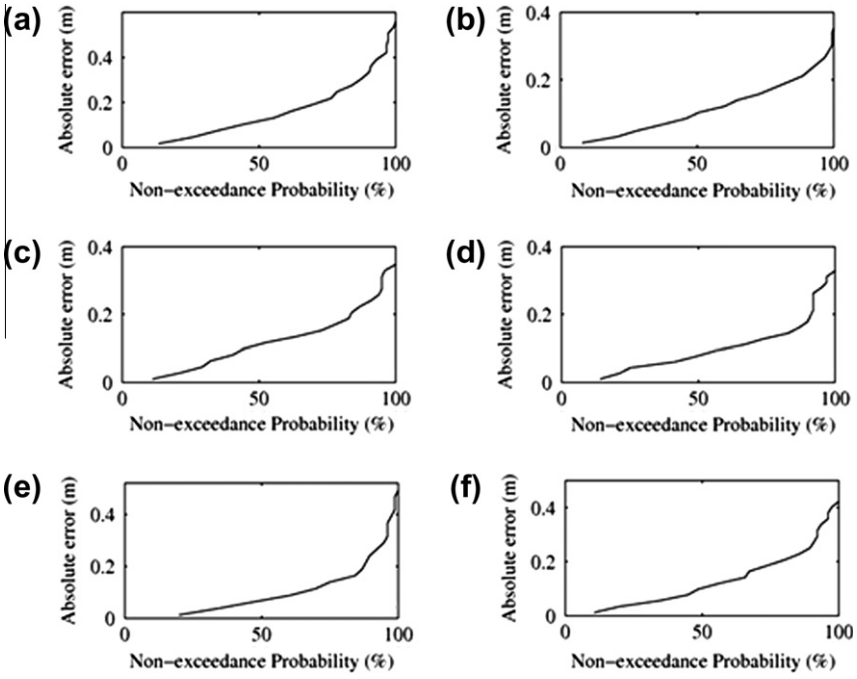

Fig. 8. Non-exceedance probability plot of absolute error in computation of water stage for a representative site in (a) woodland, (b) wooded grassland, (c) closed shrubland, (d) open shrubland, (e) grassland, and (f) cropland.

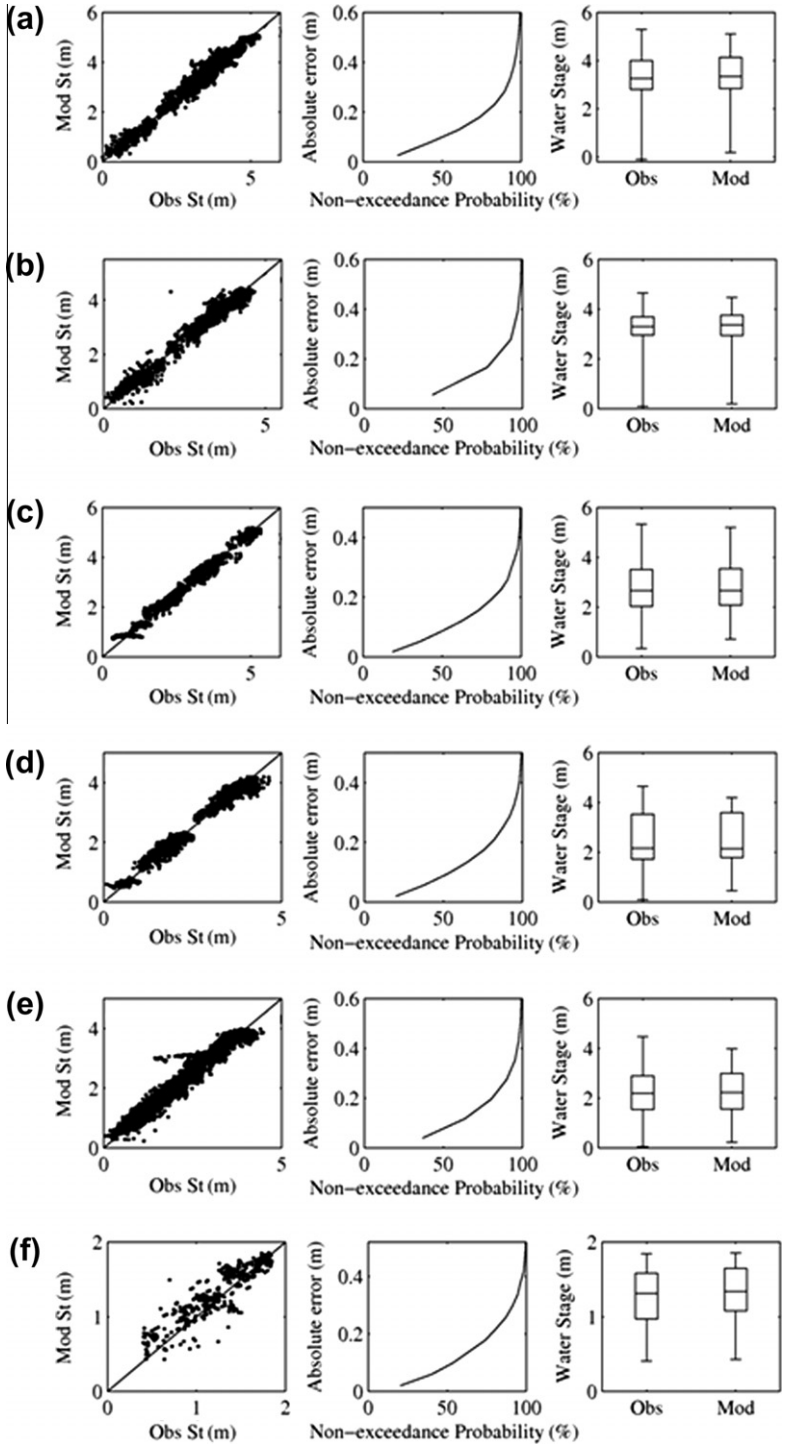

Fig. 9. Combined scatterplot, non-exceedance probability plot, and boxplot distribution of observed and modeled water stage for all the sites in (a) woodland, (b) wooded grassland, (c) closed shrubland, (d) open shrubland, (e) grassland, and (f) cropland.

of 15 cm or less and 96.8% of the estimates have an error of 30 cm or less. The Fig. 8e shows that in grasslands, 77.3% of the model estimates have 15 cm or less error and 92.1% of the estimates have 30 cm or less error. In croplands, these numbers are 60.0% for an error of 15 cm or less and 92.2% for an error of 30 cm or less [Fig. 8f].

The combined plots of scatterplot, non-exceedance probability and boxplot for all the sites in each of the six landuses have been shown in Fig. 9. For wooded grassland landuse, the combined plots for 20 sites have been shown in Fig. 9b. The combined scatterplot shows that majority of the data points lie along the 45° line with R ranging between 0.54–0.93 and RMSE = 19.8 cm; and 93.7% of the water level estimates have an absolute error of 30 cm or less. Similarly, the model captures the observed water stage variation for 15 sites in closed shrubland as shown in Fig. 9c with R ranging between 0.55–0.96 and RMSE = 16.1 cm. From the scatterplot of 17 sites in open shrubland shown in Fig. 9d, it can be seen that R ranges between 0.57–0.84 and RMSE = 17.3 cm. The combined

Table 3
Model parameters and performance for various landuse types with and without NDVI.

Landuse	Without NDVI				With NDVI				
	μ_s (m)	**T** (m/dB)	*R*	RMSE (cm)	μ_s (m)	**T** (m/dB)	**P** (m)	*R*	RMSE (cm)
Woodland	4.74	0.14	0.93	21.3	4.74	0.14	−0.08	0.94	21.3
Wooded grassland	3.30	0.07	0.89	14.3	3.30	0.07	0.04	0.89	14.3
Closed shrubland	3.94	0.09	0.86	15.5	3.94	0.09	−0.36	0.86	15.5
Open shrubland	3.48	0.08	0.84	12.8	3.48	0.08	−0.05	0.84	12.8
Grassland	1.90	0.13	0.85	15.8	1.90	0.13	−0.53	0.86	15.8
Cropland	1.82	0.14	0.79	18.0	1.82	0.14	−0.39	0.81	18.0

non-exceedance probability plot shows that 70.0% of the water levels estimates have an error of 15 cm or less and 93.2% of the estimates have an error of 30 cm or less.

The boxplot distribution shows that the model works for most of the data except for the high water stage values represented by 95th percentile and low water stage represented by 5th percentile. The combined results of the model over 36 grassland sites are summarized in Fig. 9e. The model works with *R* ranging between 0.57–0.85 and RMSE = 20.1 cm. The non-exceedance probability plot for grassland shows that 92.1% of the water stage estimates have an error of 30 cm or less. Lowering of water stage in grassland exposes the grass and most of the backscatter obtained by the TRMMPR is from the vegetated surface. On the other hand, high stage values submerge the grass and render the surface as smooth, which decreases the amount of backscatter as most of the incident radiation is specularly reflected from the water surface. There are only 4 water stage measuring sites in cropland, and for combined results, *R* ranges between 0.69–0.79 and RMSE = 18.2 cm [Fig. 9f]. In this case, 67.3% of the estimates have an error of 15 cm or less and 91.9% of the estimates have error of 30 cm or less. Water stage in cropland ranges from 0.3 m to 1.8 m. This keeps the vegetation under partial submergence, which affects the backscatter measurements.

The model that includes NDVI is compared with the model without NDVI. The model calibration parameters and model assessment parameters for two scenarios, with NDVI and without NDVI, are compared in Table 3 for a representative location in each landuse type. Model calibration and assessment parameters are the same for both cases for most landuse types, with the exception of cropland where *R* slightly increases with inclusion of NDVI in the model. This difference is due to changes in croplands due to agricultural practices such as irrigation and the stage of the crop.

NDVI is an index that measures the greenness of vegetation. The greenness is strongly linked to cropland but has a weak link with woodland, wooded grassland, and shrubland. In the case of cropland, physical changes are brought about by the crop cycle of seeding and harvesting which changes the geometrical characteristics of the cropland. There is a greater variation in greenness of cropland throughout the year as compared to other landuse types. In woodland, wooded grassland, and shrubland, the vegetation remains same for the entire year. Hence, it is seen that NDVI impacts the results for cropland but not for other landuse types.

5. Discussion

The summary of results in Table 2 shows that most of the landuses have a high correlation value except for cropland. The RMSE ranges between 16 cm and 20 cm. It is also noted that croplands are not flooded all the time. Thus, under dry and field capacity conditions, the modeled backscatter is not dependent on partial submergence; it depends on soil moisture and vegetation condition. The lower accuracy of the model in cropland can be attributed to the intermittent flooding of these areas. Results show that the model works reasonably well for all landuses in the study area.

For woodland vegetation (height >5 m), fluctuation of water depth primarily affects the exposure of the lower canopies and for trees, the lower parts of the canopies. The partial submergence of woodland vegetation affects the backscatter by exhibiting high backscatter for higher stage values and low backscatter for low stage values.

The results show that the model over-estimates the low stage values in relatively dense vegetation. This is attributable to the shorter wavelength of TRMMPR waves that are attenuated by the vegetation canopy. In tall and dense vegetation with low water stage levels, the backscatter has little sensitivity to the variations in water stage.

The proposed model depends on the height of the exposed vegetation under varying water stage. It would be difficult to calibrate the model over areas where water stage temporal variations are negligible. The model performance deteriorates where vegetation remains under water for extended periods of time or where most of the vegetation is submerged. Under such conditions the specular reflection of the water surface dominates, making it difficult to capture the variations due to the exposed vegetation.

This research shows the relationship between the TRMMPR backscatter measurements and water stage. The proposed model uses ground measurements for calibration over a given landcover type. The calibrated model can be used to estimate water stage from backscatter measurement over that landcover. Although NDVI does not show much contribution in this model, Leaf Area Index (LAI), a relatively better measure of vegetation density, may improve results. The model performance deteriorates with the reduction of vegetation over free water. In the case of completely inundated vegetation, the model does not work because of the specular reflection of incident energy from the water surface. The model also does not work in extreme dry conditions.

The simple model proposed and tested in this paper suggests that changes in water stage alter the backscattering coefficient measured by the radar. The ability to estimate water stage from the measured backscatter depends upon the type of vegetation cover. In relatively taller vegetation, where the stature of the vegetation above water is sufficient, the changes in water stage are estimated from the backscatter. With reduction in the vegetation height, the relative proportion of the vegetation above water reduces and impacts the accuracy of estimated water stage. Moreover, in the cropland, the stage of crop and cycle of flooding and drying makes it difficult for the model to estimate water stage accurately. Nevertheless, the results indicate that the TRMMPR backscatter measurements can be used to estimate the water stage.

6. Conclusions

A simple empirical model is developed that relates water stage to TRMMPR backscatter measurements. Backscatter depends on the dielectric and physical characteristics of the target area. Its

dependence on the partial submergence of vegetation is used as the basis of estimation of water stage from σ° measurements.

The model works reasonably well over various landuse types in wetlands of South Florida. For various landuse types, the correlation between observed and modeled water stage ranges between 0.54–0.96 and root mean square error ranges between 16.1 cm and 20.1 cm. A high correlation and low root mean square error shows the strength of the model.

A model relating water stage to TRMMPR backscatter and NDVI is also developed and tested. NDVI accounts for vegetation greenness, and it improves the model performance for cropland. This happens because NDVI has a strong link with the geometrical characteristics of the cropland and these characteristic change due to the crop cycles and seasons of seeding and harvesting of crops. Over the other landuse types that are characterized by tall trees and shrubs, inclusion of NDVI in the model does not improve the results. This occurs because there is not much variation in vegetation growth from one season to the other. This research provides a method to compliment the ground measurements of water stage using spaceborne backscatter measurements. It provides a novel use of TRMMPR data and gives an insight into the effect of water level in partially inundated vegetation on radar backscatter.

Acknowledgements

The funding for this work was provided by National Oceanic and Atmospheric Administration's Social Application and Research Program (NOAA-SARP) Award NA070AR4310324.

References

Ahmad, S., Simonovic, S.P., 2001. Integration of heuristic knowledge with analytical tools for selection of flood control measures. Canadian Journal of Civil Engineering 28 (2), 208–221.

Ahmad, S., Kalra, A., Stephen, H., 2010. Estimating soil moisture using remote sensing data: a machine learning approach. Advances in Water Resources 33 (1), 69–80.

Alaa, A., Abtew, W., Horn, S.V., Khanal, N., 2000. Temporal and spatial characterization of rainfall over central and south Florida. Journal of the American Water Resources Association 36 (4), 833–848.

Alsdorf, D., Lettenmaier, D., Vörösmarty, C., The NASA Surface Water Working Group, 2003. The need for global, satellite-based observations of terrestrial surface waters. EOS Transactions of AGU 84 (269), 275–276.

Birkett, C.M., Mertes, L.A.K., Dunne, T., Costa, M., Jasinski, J., 2002. Altimetric remote sensing of the Amazon: application of satellite radar altimetry. Journal of Geophysical Research 107 (D20), 8059. doi:10.1029/2001JD000609.

Bourgeau-Chavez, L.L., Smith, K.B., Brunzell, S.M., Kasischke, E.S., Romanowicz, E.A., Richardson, C.J., 2005. Remote monitoring of regional inundation patterns and hydroperiod in the greater everglades using synthetic aperture radar. Wetlands 25 (1), 176–191.

Brande, J., 1980. Worthless, valuable, or what – an appraisal of wetlands. Journal of Soil and Water Conservation 35 (1), 12–16.

Calmant, S., Seyler, F., Cretaux, J.F., 2008. Monitoring continental surface water by satellite altimetry. Survey of Geophysics 29, 247–269. doi:10.1007/s10712-008-9051-1.

Cavender, J.C., Raper, K.B., 1968. The occurrence and distribution of Acrasieae in forests of subtropical and tropical America. American Journal of Botany 55 (4), 504–513.

Doren, R.F., Rutchey, K., Welch, R., 1999. The Everglades: a perspective on the requirements and applications for vegetation map and database products. Photogrammetric Engineering and Remote Sensing 65 (2), 155–161.

Gao, F., Jin, Y.F., Li, X.W., Schaaf, C.B., Strahler, A.H., 2002. Bidirectional NDVI and atmospherically resistant BRDF inversion for vegetation canopy. IEEE Transactions on Geoscience and Remote Sensing 40 (6), 1269–1278.

Gorham, E., Dean, W.E., Sanger, J.E., 1983. The chemical-composition of lakes in the north-central United-States. Limnology and Oceanography 28 (2), 287–301.

Hansen, M.C., DeFries, R.S., Townshend, J.R.G., Sohlberg, R., 2000. Global land cover classification at 1 km spatial resolution using a classification tree approach. International Journal of Remote Sensing 21, 1331–1364.

Hong, S.H., Wdowinski, S., Kim, S.W., 2010. Evaluation of TerraSAR-X observations for wetland InSAR application. IEEE Geosciences and Remote Sensing 48, 864–873.

Hong, S.H., Wdowinski, S., Kim, S.W., in press. Space-based multi-temporal monitoring of wetland water levels: case study of WCA1 in the Everglade, Remote Sensing for Environment.

Johnson, W.C., Boettcher, S.E., Poiani, K.A., Guntenspergen, G., 2004. Influence of weather extremes on the water levels of glaciated prairie wetlands. Wetlands 24 (2), 385–398.

Kasischke, E.S., Bourgeau-Chavez, L.L., 1997. Monitoring south florida wetlands using ERS-1 SAR imagery. Photogrammetric Engineering and Remote Sensing 63 (3), 281–291.

Kasischke, E.S., Smith, K.B., Bourgeau-Chavez, L.L., Romanowicz, E.A., Brunzell, S., Richardson, C.J., 2003. Effects of seasonal hydrologic patterns in south Florida wetlands on radar backscatter measured from ERS-2 SAR imagery. Remote Sensing of Environment 88 (4), 423–441.

Kozu, T., Kawanishi, T., Kuroiwa, H., Kojima, M., Oikawa, K., Kumagai, H., et al., 2001. Development of precipitation radar onboard the tropical rainfall measuring mission (TRMM) satellite. IEEE Transactions on Geoscience and Remote Sensing 39 (1), 102–116.

Kummerow, C., Barnes, W., Kozu, T., Shiue, J., Simpson, J., 1998. The tropical rainfall measuring mission (TRMM) sensor package. Journal of Atmospheric and Oceanic Technology 15 (3), 809–817.

Li, L., Im, E., Connor, L.N., Chang, P.S., 2004. Retrieving ocean surface wind speed from the TRMM precipitation radar. IEEE Transactions on Geoscience and Remote Sensing 42 (6), 1271–1282.

Mason, D.C., Horritt, M.S., Dall' Amico, J.T., Scott, T.R., Bates, P.D., 2007. Improving river flood extent delineation from synthetic aperture radar using airborne laser altimetry. IEEE Transactions on Geoscience and Remote Sensing 45 (12), 3932–3943.

McAllister, L.S., Peniston, B.E., Leibowitz, S.G., Abbruzzese, B., Hyman, J.B., 2000. A synoptic assessment for prioritizing wetland restoration efforts to optimize flood attenuation. Wetlands 20 (1), 70–83.

Mertes, L.A.K., Daniel, D.L., Melack, J.M., Nelson, B., Martinelli, L.A., Forsberg, B.R., 1995. Spatial patterns of hydrology, geomorphology, and vegetation on the floodplain of the Amazon river in Brazil from a remote sensing perspective. Geomorphology 13 (1–4), 215–232.

Mosquera-Machado, S.C., Ahmad, S., 2007. Flood hazard assessment of Atrato river in Colombia. Water Resources Management 21, 591–609.

Narayan, U., Lakshmi, V., Jackson, T., 2006. A simple algorithm for spatial disaggregation of radiometer derived soil moisture using higher resolution radar observations. IEEE Transactions on Geoscience and Remote Sensing 44 (6), 1545–1554.

Ozesmi, S.L., Bauer, M.E., 2002. Satellite remote sensing of wetlands. Wetlands Ecology and Management 10 (5), 381–402.

Pant, H.K., Rechcigl, J.E., Adjei, M.B., 2003. Carbon sequestration in wetlands: concept and estimation. Journal of Food Agriculture and Environment 1 (2), 308–313.

Richards, J.A., Woodgate, P.W., Skidmore, A.K., 1987. An explanation of enhanced radar backscattering from flooded forests. International Journal of Remote Sensing 8 (7), 1093–1100.

Satake, M., Hanado, H., 2004. Diurnal change of Amazon rain forest – observed by Ku-band spaceborne radar. IEEE Transactions on Geoscience and Remote Sensing 42 (6), 1127–1134.

Seto, S., Oki, T., Musiake, K., 2003. Surface soil moisture estimation by TRMM/PR and TMI. In: Proceedings of International Geoscience and Remote Sensing Symposium, vol. III, pp. 1960–1962.

Sippel, S.J., Hamilton, S.K., Melack, J.M., Novo, E.M.M., 1998. Passive microwave observations of inundation area and the area/stage relation in the Amazon River floodplain. International Journal of Remote Sensing 19 (16), 3055–3074.

Stephen, H., Long, D.G., 2002. Multi-spectral analysis of the Amazon basin using Seawinds, ERS, NASA, Seasat Scatterometer, TRMM-PR and SSM/I. In: Proceedings of International Geoscience and Remote Sensing Symposium, vol. 5, Toronto, Canada, pp. 2808–2810.

Stephen, H., Long, D.G., 2005. Microwave backscatter modeling of erg surfaces in the Sahara desert. IEEE Transactions on Geoscience and Remote Sensing 43 (2), 238–247.

Stephen, H., Ahmad, S., Piechota, T.C., Tang, C., 2010. Relating surface backscatter response from TRMM precipitation radar to soil moisture: results over a semi-arid region. Hydrology and Earth System Sciences 14, 193–204.

Tucker, C.J., 1979. Red and photographic infrared linear combinations for monitoring vegetation. Remote Sensing of Environment 8 (2), 127–150.

Ulaby, F.T., Batlivala, P.P., 1976. Optimum radar parameters for mapping soil-moisture. IEEE Transactions on Geosciences and Remote Sensing 14 (2), 81–93.

Vedwan, N., Ahmad, S., Miralles-Wilhelm, F., Broad, K., Letson, D., Podesta, G., 2008. Institutional evolution in Lake Okeechobee Management in Florida: characteristics, impacts, and limitations. Water Resources Management 22, 699–718.

Wdowinski, S., Amelung, F., Miralles-Wilhelm, F., Dixon, T., Carande, R., 2004. Space-based measurements of sheet-flow characteristics in the Everglades wetland, Florida. Geophysical Research Letters 31, L15503.

Wdowinski, S., Kim, S.W., Amelung, F., Dixon, T.H., Miralles-Wilhelm, F., Sonenshein, R., 2008. Space-based detection of wetlands' surface water level changes from L-band SAR interferometry. Remote Sensing of Environment 112 (3), 681–696.

Zhang, B., 2008. Data Mining, GIS and Remote Sensing: Application in Wetland Hydrological Investigation. Ohio State University, Ohio.